Porosity and Biocompatibility Study of Ceramic Implants Based on ZrO_2 and Al_2O_3

Larisa Litvinova[1, a)], Valeria Shupletsova[1, b)], Vladimir Leitsin[1, c)], Roman Vasyliev[2, d)], Dmitry Zubov[2, e)], Ales Buyakov[3, 4, 5, f)], and Sergey Kulkov[3, 4, 5, f)]

[1] *Immanuel Kant Baltic Federal University, Kaliningrad, Russia*
[2] *State Institute of Genetic and Regenerative Medicine, National Academy of Medical Sciences of Ukraine, Kiev, Ukraine*
[3] *Institute of Strength Physics and Materials Science SB RAS, Tomsk, 634055, Russia*
[4] *National Research Tomsk State University, Tomsk, 634050, Russia*
[5] *National Research Tomsk Polytechnic University, Tomsk, 634050, Russia*

[a)] Corresponding author: larisalitvinova@yandex.ru
[b)] vshupletsova@mail.ru
[c)] leitsin@mail.ru
[d)] rvasiliev@ukr.net
[e)] zoubov77@yahoo.com
[f)] kulkov@ms.tsc.ru

Abstract. The work studies $ZrO_2(Me_xO_y)$-based porous ceramics produced from the powders consisting of hollow spherical particles. It was shown that the structure is represented by a cellular framework with bimodal porosity consisting of sphere-like large pores and pores that were not filled with the powder particles during the compaction. For such ceramics, the increase of pore volume is accompanied by the increased strain in an elastic area. It was also shown that the porous ZrO_2 ceramics had no acute or chronic cytotoxicity. At the same time, ceramics possess the following osteoconductive properties: adhesion support, spreading, proliferation and osteogenic differentiation of MSCs.

INTRODUCTION

Porous ceramic materials have been successfully used in various fields, including heat-insulating construction materials, because they are durable, corrosion resistant and they possess stable thermal features [1–3]. Porous ceramics are also a promising material for medical use in the field of traumatology and orthopedics for critical sized bone defect recovery. Thus porous ceramics can act both as osteoplastic material and as 3D scaffold for tissue-engineered bone equivalent modeling [4].

Ceramics based on partially stabilized zirconium are the most interesting among the variety of ceramic materials due to their inherent high transformation toughening. It is known that the characteristics are determined by the quality of source ceramic powder (particle shape, particle size distribution), the compaction conditions, sintering mode, features of each phase and how these phases, including pores, are arranged in relation to each other. The most important factor in the successful application of materials is understanding the features of their structure and their behavior under mechanical impact.

The aim of a paper is to examine the pore structure of $ZrO_2(Me_xO_y)$ ceramics and its biocompatibility with multipotent stromal cells (mesenchymal stem cells, MSCs) by *in vitro* assays.

International Conference on Physical Mesomechanics of Multilevel Systems 2014
AIP Conf. Proc. 1623, 347-350 (2014); doi: 10.1063/1.4898953

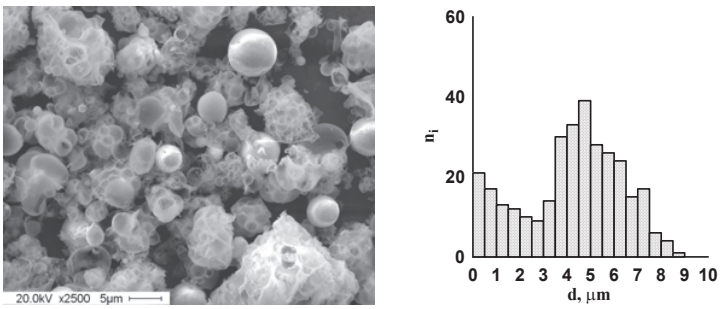

(a) (b)

FIGURE 1. Plasmachemically-synthesized ZrO_2 powders: (a) SEM-image of plasmachemically-synthesized $ZrO_2(Y_2O_3)$ powder, (b) particle size distribution of $ZrO_2(Y_2O_3)$ powder

MATERIALS AND EXPERIMENTAL PROCEDURE

The materials for the study were ceramics obtained from ZrO_2(MgO) and $ZrO_2(Y_2O_3)$ powders produced by liquid-phase decomposition of precursors synthesized in high-frequency discharge plasma (the plasmachemical method).

Porous ceramic ZrO_2(MgO) and $ZrO_2(Y_2O_3)$ samples were prepared by compacting and subsequent sintering of compacts at the homologous temperatures ranging from 0.63 to 0.56 during the isothermal soaking for 1 to 5 hours. The porosity of ZrO_2(MgO) and $ZrO_2(Y_2O_3)$ ceramics ranged from 15% to around 45% and from 30% to 80%, respectively. X-ray studies were carried out using a diffractometer with a CuKα source of filtered radiation. The studies on the ceramic structure were carried out using Philips SEM 515 scanning electron microscope.

To assess the biocompatibility of porous ceramics, the adipose-derived MSCs have been used. MSCs were isolated by enzymatic method and cultured in DMEM:F12 supplemented with 2 mM *L*-glutamine and 10% FBS ("Sigma", USA) and incubated with the use of Cell IQ® v2 MLF integrated continuous live cell imaging and analysis platform (CM Technologies). The third passage MSCs have been used for the experiments. Preliminarily, MSC culture compliance with minimal criteria was made for phenotype (flow cytometry) and differentiation potential (differentiation assays for adipocytes and osteoblasts) [5]. Prior to seeding over the implants, cell viability in suspension was assessed by Trypan blue staining. [6] To assess the cytotoxicity of the implants and the viability of cultured MSCs over their surfaces, cell combined double staining with fluorescein diacetate (FDA) and propidium iodide (PI) 24h after inoculation and 7 days after culturing was made [7]. Assessment of cytotoxicity was performed using Axio Observer A1 inverted fluorescent microscope (Carl Zeiss, Germany). For the further biocompatibility assessment, the MSC osteogenic differentiation assay was performed according to standard protocols [8]. MSCs were cultured in implants or over its surface for 14 days, followed by detection of alkaline phosphatase activity using the BCIP/NBT substrate (Sigma, USA) [9].

RESULTS AND DISCUSSION

Powders. Figure 1(a) represents the SEM-picture of plasmachemically-synthesized ZrO_2 powder (3 mol.% Y_2O_3) and the powder particle size distribution. ZrO_2 (3 mol.% MgO) and ZrO_2 (3 mol.% Y_2O_3) powders practically have no difference in morphological structure and they consist of hollow particles of a spherical shape and a large number of units having no regular form. The average particle size of the spherical ZrO_2(MgO) and $ZrO_2(Y_2O_3)$ powders was 1.8 and 1.5 μm, respectively.

The phase composition of $ZrO_2(Y_2O_3)$ powder includes tetragonal and monoclinic ZrO_2. The ZrO_2(MgO) powder comprised the cubic, tetragonal and monoclinic phases of ZrO_2. The fraction of tetragonal ZrO_2 in $ZrO_2(Y_2O_3)$ powder amounted about 95%, while that of cubic ZrO_2 in ZrO_2(MgO) powder was 75%. The average size of the coherent scattering regions (CSR) of tetragonal ZrO_2 in $ZrO_2(Y_2O_3)$ powder was 20 nm, and for the monoclinic modification it was 50 nm. The average size of CSR for cubic modification of ZrO_2 in ZrO_2(MgO) powder was 20 nm, for monoclinic ZrO_2 it was 30 nm and for the tetragonal phase it was 15 nm.

Sintered ceramics. Figure 2(a) represents the SEM-image of $ZrO_2(Y_2O_3)$ ceramic structure and the pore size distribution. The structure of ZrO_2(MgO) and $ZrO_2(Y_2O_3)$ ceramics was represented by a cellular frame.

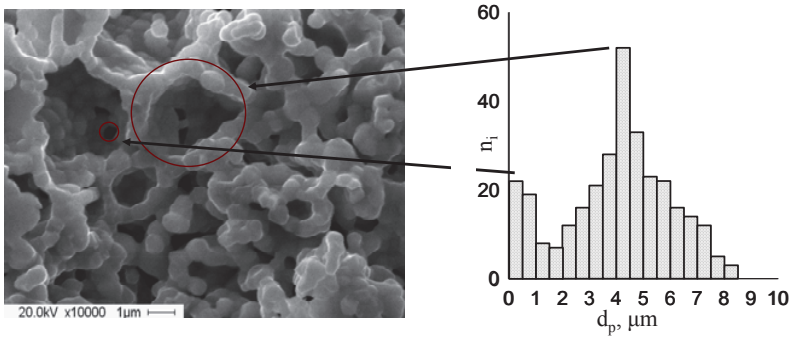

FIGURE 2. SEM-Picture of ZrO_2 ceramics structure (Y_2O_3), the characteristic pore size distribution of ZrO_2 ceramics (MgO) with a porosity of ≈40%

The cells were nearly spherical and the cell size exceeded many-fold the thickness of walls that were represented by a single-layer stack of ZrO_2 grains. The pore size distribution was bimodal. The first maximum was formed by equiparticle pores, the voids that were not filled with powder particles during the compaction, and the second maximum was conditioned by the larger pores with a shape close to spherical. The plots presented in Fig. 2b demonstrates the dependence of the average size of equiparticle and large spherical pores on the porosity in ZrO_2(MgO) and ZrO_2(Y_2O_3) ceramics. It is clear that the increase of pore volume in the material from about 30 to 80% achieved by reducing the sintering temperature of the samples was accompanied by the increase of the average size of large pores from 2 to 6 microns. Changing the porosity of the material had practically no effect on the average size of equiparticle pores having the average size of 0.5 microns. It can be assumed that the presence of large pores close to a spherical shape in the ceramics is conditioned by the presence of hollow spherical particles in the source powders, since their average size is commensurate with the average size of large pores occurring in the sintered material.

Biocompatibility: cytotoxicity and osteogenic differentiation of MSCs/ Cultured adipose tissue-derived MSCs used for the preliminary assessment of the biocompatibility of porous ceramic implants had the capacity to differentiate in adipogenic and osteogenic directions and had the following phenotype: CD73+ CD90+ CD105+ and CD34- CD45-. Combined staining of FDA/PI cells cultured on the surface or in the implants showed no cytotoxicity of porous ZrO_2 ceramics (Fig. 3). The results of the cell viability evaluation in suspension with the use of Trypan blue staining before seeding and 24h after culturing on implants by staining with FDA/PI exhibited similar values (suspension, Trypan blue, 96.42% ± 1.8% viable cells; implant, FDA/PI, 93.78% ± 2.15%). Microscopic observation showed that MSCs 24h after seeding adhered to the surface of the implant and generated intensive and uniform green FDA stain in the absence of red PI stain, which indicates a high metabolic activity of the cells and the integrity of their membrane. At the same time the cells had different spreading degree due to the rough surface of the implant through its physical structure (the presence of pores and composition of hollow particles of a spherical shape and a large number of units having no regular form).

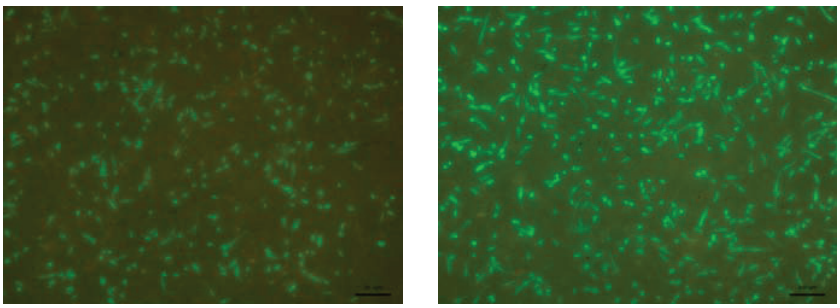

(a) (b)

FIGURE 3. Viability assessment of MSCs cultured on the porous surface of the ZrO_2 ceramic implants: (a) 24h of culturing and (b) 7 days of culturing. Combined FDA/PI stain

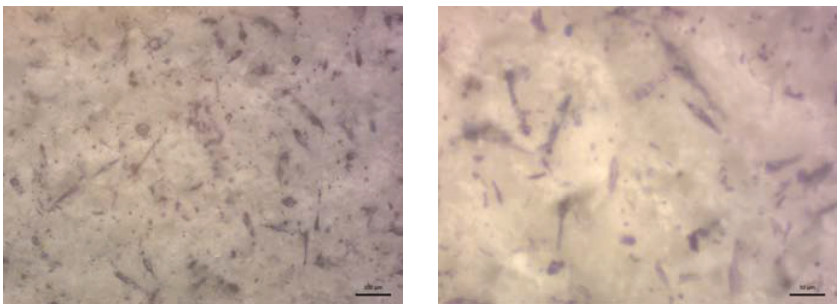

(a) (b)

FIGURE 4. Detection of alkaline phosphatase activity after osteogenic differentiation of MSCs cultured on the porous ZrO_2 ceramic implants. BCIP/NBT stain

Cell viability after 7 days of culturing with porous ZrO_2 ceramic implants was 92.56% ± 1.44%, which is comparable to cell viability before seeding and after 24h culturing with implants (difference is not statistically significant). Moreover, after 7 days of MSC culturing on the surface of porous ZrO_2 ceramics, the formation of cell clusters due to their proliferation was noted. Thus, porous ZrO_2 ceramic implants do not have the acute and chronic cytotoxicity. Detection of alkaline phosphatase activity with use of BCIP/NBT substrate showed that cultured MSCs on the porous surface of ZrO_2 ceramic implant retain their ability for osteogenic differentiation (Fig. 4). Based on the results of the osteogenic differentiation of MSCs, we can conclude that porous ZrO_2 ceramic implants possess osteoconductive properties.

CONCLUSIONS

It was elucidated that the structure of $ZrO_2(Me_xO_y)$ ceramics made of powders consisting of hollow spherical particles with the porosity of 30% is represented by a cellular framework with the bimodal porosity, formed by large pores with the shape close to spherical and pores that were not filled with the powder particles during the compaction. It was found that $ZrO_2(Me_xO_y)$ ceramics with bimodal pore size distribution at the porosity exceeding 30% demonstrate the micromechanical instability during the compaction, which is caused by the reversible deformation of the cellular elements. For the cases of such ceramics the increase of pore volume is accompanied by the increase of strain in the elastic area. It was also shown that the porous ZrO_2 ceramics had no acute or chronic cytotoxicity. At the same time, the porous ZrO_2 ceramics possess the osteoconductive properties: adhesion support, spreading, proliferation and osteogenic differentiation of MSCs.

This work has been financial supported by Competitiveness Improvement Program of the Tomsk State University, the Foundation Program of Siberian Branch RAS and RF Ministry of Education and Science (Agreement No. 14.607.21.0069).

REFERENCES

1. L. A. Gomze and L. N. Gomze, IOP Conf. Ser. Mater. Sci. Eng. **47** (2013).
2. S. Kulkov, V. Maslovskii, and S. Buyakova, Russ. J. Appl. Phys. **47**(3), 320–324 (2002).
3. E. Kalatur, A. Kozlova, S. Buyakova, and S. Kulkov, "Deformation behavior of zirconia-based porous ceramics", IOP Conf. Ser. Mater. Sci. Eng. **47** (2013).
4. J. Will, R. Melcher, C. Treul, N. Travitzky, U. Kneser, E. Polykandriotis, R. Horch, and P. Greil, J. Mater. Sci. Mater. Med. **19**, 2781–2790 (2008).
5. M. Dominici, K. Le Blanc, I. Mueller, I. Slaper-Cortenbach, F. Marini, D. Krause, R. Deans, A. Keating, D. Prockop, and E. Horwitz, Cytotherapy **8**, 315–317 (2006).
6. R. I. Freshney, *Culture of Animal Cells: A Manual of Basic Technique and Specialized Applications* (Wiley-Blackwell, New Jersey, 2010).
7. S. Johnston, V. Nguyen, and D. Coder, Curr. Protoc. Cytom. **64**, 9.2.1–9.2.26 (2013).
8. D. Prockop, D. Phinney, and B. Bunnel, *Mesenchymal Stem Cells: Methods And Protocols* (Humana Press, Totowa, NJ, 2008).
9. J.-D. Jang, S.-J. Kim, H.-M. Yoon, and D.-Ch. Shin, Tissue Eng. Regenerat. Med. **8**, 371–379 (2011).